Organic & Biomolecular Chemistry

ROYAL SOCIETY OF CHEMISTRY

PAPER

View Article Online
View Journal | View Issue

Cite this: *Org. Biomol. Chem.*, 2021, **19**, 3241

Design, synthesis, and evaluation of positron emission tomography/fluorescence dual imaging probes for targeting facilitated glucose transporter 1 (GLUT1)†

Richard Yuen,[a,b] Michael Wagner,[b] Susan Richter,[b] Jennifer Dufour,[b] Melinda Wuest,[b,c] Frederick G. West[a,c] and Frank Wuest *[a,b,c]

Increased energy metabolism followed by enhanced glucose consumption is a hallmark of cancer. Most cancer cells show overexpression of facilitated hexose transporter GLUT1, including breast cancer. GLUT1 is the main transporter for 2-deoxy-2-[^{18}F]fluoro-D-glucose (**2-[^{18}F]FDG**), the gold standard of positron emission tomography (PET) imaging in oncology. The present study's goal was to develop novel glucose-based dual imaging probes for their use in tandem PET and fluorescence (FI) imaging. A glucosamine scaffold tagged with a fluorophore and an ^{18}F-label should confer selectivity to GLUT1. Out of five different compounds, 2-deoxy-2-((7-sulfonylfluoro-2,1,3-benzoxadiazol-4-yl)amino)-D-glucose (**2-FBDG**) possessed favorable fluorescent properties and a similar potency as 2-deoxy-2-((7-nitro-2,1,3-benzoxadiazol-4-yl)amino)-D-glucose (2-NBDG) in competing for GLUT1 transport against **2-[^{18}F]FDG** in breast cancer cells. Radiolabeling with ^{18}F was achieved through the synthesis of prosthetic group 7-fluoro-2,1,3-benzoxadiazole-4-sulfonyl [^{18}F]fluoride ([^{18}F]FBDF) followed by the reaction with glucosamine. The radiotracer was finally analyzed *in vivo* in a breast cancer xenograft model and compared to **2-[^{18}F]FDG**. Despite favourable *in vitro* fluorescence imaging properties, **2-[^{18}F]FBDG** was found to lack metabolic stability *in vivo*, resulting in radiodefluorination. Glucose-based **2-[^{18}F]FBDG** represents a novel dual-probe for GLUT1 imaging using FI and PET with the potential for further structural optimization for improved metabolic stability *in vivo*.

Received 2nd February 2021,
Accepted 22nd March 2021

DOI: 10.1039/d1ob00199j

rsc.li/obc

Introduction

Non-invasive cancer imaging is an essential tool in precision medicine for accurate diagnosis and monitoring of treatment responses.[1] In recent years, the combination of different molecular imaging modalities and the development of dual-functionality imaging probes has significantly advanced the field of precision medicine in oncology and beyond.[2–4] Positron emission tomography (PET) is a routine nuclear medicine technique that offers detection of metabolic and physiological processes with high sensitivity.[5] Complementary to PET, fluorescence (FI) imaging relies on stable fluorophores, which allows for longitudinal imaging as PET radiotracers involve the use of radioisotopes with relatively short decay half-lives (^{18}F $t_{1/2}$ = 109.8 min). The development of dual-probes capable of both PET and FI imaging would combine the advantages of both imaging techniques to improve patient care and outcomes.[6–8] Utilizing a single imaging agent for both PET and FI detection, rather than using two separate probes, will ensure no differences in biodistribution, resulting in a high correlation between the two imaging techniques.[2] In the clinic, solid tumour management would benefit from the accurate detection of the tumour with PET, followed by fluorescence-guided surgical resection of the tumour mass. For practical purposes in the clinic, the patient would first be administered the radiolabeled dual-probe for PET imaging. Then, the patient is administered the non-radioactive dual-probe prior to surgery to enable FI. This two-dose strategy would usually be required as the radioactive compound is administered in trace amounts. A first-in-human study in 2018 demonstrated the feasibility of PET and optical dual-modality image-guided surgery using ^{68}Ga-IRDye800CW-bombesin in

[a]*Department of Chemistry, 11227 Saskatchewan Drive University of Alberta, Edmonton, AB, Canada T6G 2G2. E-mail: wuest@ualberta.ca; Fax: +780-432-8483; Tel: +780-989-8150*
[b]*Department of Oncology, Cross Cancer Institute, University of Alberta, Edmonton, AB, Canada T6G 1Z2*
[c]*Cancer Research Institute of Northern Alberta, University of Alberta, Edmonton, AB, Canada T6G 2S2*

†Electronic supplementary information (ESI) available. See DOI: 10.1039/d1ob00199j

glioblastoma.[9] The unrivalled sensitivity of PET and the capability to visualize tumour margins through FI will allow for precise targeting and better patient outcomes by removing critical tumour margins during tumour resection while minimizing damage to healthy tissue.[10] This technique is particularly beneficial for the surgical removal of solid tumours where visual differentiation between tumour tissue and healthy tissue is difficult, as frequently observed in breast cancers.[10]

One of the hallmarks of cancer is the Warburg effect or the dysregulation of cellular energy metabolism.[11] Cancer cells often require more energy than normal cells as they grow and divide at a higher rate. In cancer cells, a marked shift from mitochondrial oxidative phosphorylation to less efficient cytosolic glycolysis to synthesize adenosine triphosphate (ATP) is observed. Consequently, cancer cells are characterized by the overexpression of various facilitated hexose transporters known as GLUTs. Glucose transporter 1 (GLUT1), the primary glucose transporter, is overexpressed in many cancer cells.[12] Therefore, targeting GLUT1 as a cancer biomarker will confer selective cancer cell uptake of the imaging probe compared to normal cells. A standard method for targeting GLUT1 involves the functionalization of glucose to obtain specific GLUT1 targeting imaging agents.[13,14]

In this line, 2-deoxy-2-[^{18}F]fluoro-D-glucose (**2-[^{18}F]FDG**) represents the gold standard radiotracer for clinical PET imaging of different types of cancer.[13] Another glucose derivative, 2-deoxy-2-((7-nitro-2,1,3-benzoxadiazol-4-yl)amino)-D-glucose (2-NBDG), has been successfully used for fluorescence (FI) imaging of GLUT1 expression in cells.[14] 2-NBDG demonstrated that glucose modification at the C2 position with a moderately sizeable aromatic group does not prevent GLUT1 recognition. The need to expand on the range of available tracers is evident, given the crucial individual variability seen in cancer patients as each cancer is characterized by a different gene and protein expression profile.

Several fluorescent probes targeting GLUT1 have been published recently,[15–17] and their uptake profiles were correlated with that of **2-[^{18}F]FDG**.[18–20] Besides a few reports discussing bimodal PET/FI probes for *in vivo* oncologic and neurodegenerative disease imaging,[21–23] to date, no dual PET/FI probes targeting GLUT1 have been described.

The development of GLUT1-targeting dual-probes that contain both a fluorophore and an ^{18}F reporter is a particular challenge. The fluorophores that are used must be of reasonable size and enable facile incorporation of ^{18}F while preserving favourable fluorescent properties. Several reports described the use of large chelator molecules such as NOTA or DOTA for the radiolabeling with radiometals like ^{68}Ga and ^{64}Cu in addition to fluorescent tags to prepare bifunctional peptide and protein imaging agents.[22,24,25] However, the large fluorophore/chelator concept may not be feasible for targeting GLUT1 as the increasing steric demand would likely result in the loss of substrate recognition by the transporter. The present study aimed to design, synthesize, and screen potential fluorine-containing fluorophores for substrate recognition by GLUT1 in an *in vitro* assay.

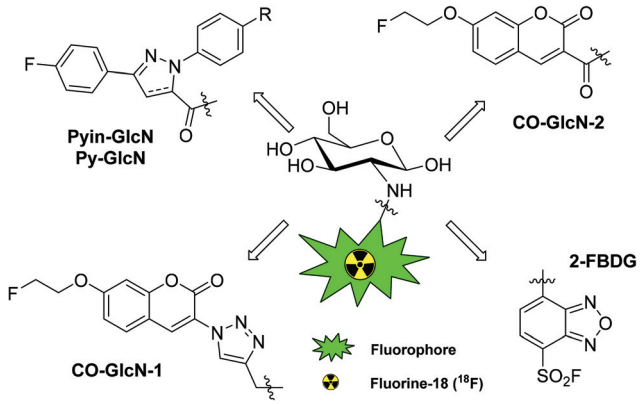

Fig. 1 Structures of the different fluorine-containing fluorophores attached to GLUT1-targeting glucosamine (center) that are presented in this work, enabling dual-probe capability (top left: diaryl-pyrazoles/pyrazolines; bottom left/top right: coumarins; bottom right: benzoxadiazoles).

The non-radioactive ^{19}F-containing fluorophores should be readily accessible, and the synthetic route to the respective ^{18}F-labelled fluorophores should be feasible. In addition to these requirements, the dual-imaging reporter motifs should readily conjugate to the glucosamine scaffold to generate the desired bimodal GLUT1 imaging probe. Herein, we have synthesized and tested novel dual-probes based on diarylpyrazoline/diarylpyrazole, coumarin, and benzoxadiazole fluorophores for their fluorescent properties as well as their potency to compete with **2-[^{18}F]FDG** for transport through GLUT1 (Fig. 1). In a second step, we have chosen **2-FBDG** for radiolabeling with ^{18}F to form **2-[^{18}F]FBDG**. **2-[^{18}F]FBDG** was tested in a breast cancer model *in vivo* as a potential dual PET/FI imaging agent.

Results and discussion

Chemistry

The synthesis of FI imaging probes **Py-GlcN** and **Pyin-GlcN** containing a diaryl-pyrazoline/diarylpyrazole fluorophore is outlined in Scheme 1. ^{19}F-Containing tetrazoles **1** and **2** were subjected to a photo-activated click reaction with acrylamide-conjugated glucosamine **3**.[22,26,27] The [3 + 2] dipolar cycloaddition between an *in situ*-generated nitrile imine and **3** generated pyrazolines **4** and **5**. During the reaction, pyrazoline **4** was susceptible to oxidation to form pyrazole **6**. Thus, oxidation with DDQ provided a single characterizable compound. Tetrazole **2** was more reactive than tetrazole **1** under irradiation with a UV light meant for visualizing TLC plates (365 nm). The substituent on the 2-phenyl group had to be sufficiently electron-donating to undergo the photo-click reaction as aryl groups with less electron-donating alkyl groups had unfavourable reaction kinetics.

However, the more electron-rich tetrazole **2** proved to be difficult to synthesize (3% yield). This was likely due to the diazonium salt undergoing electrophilic substitution with an equivalent of the parent aniline, forming the azo dye as a

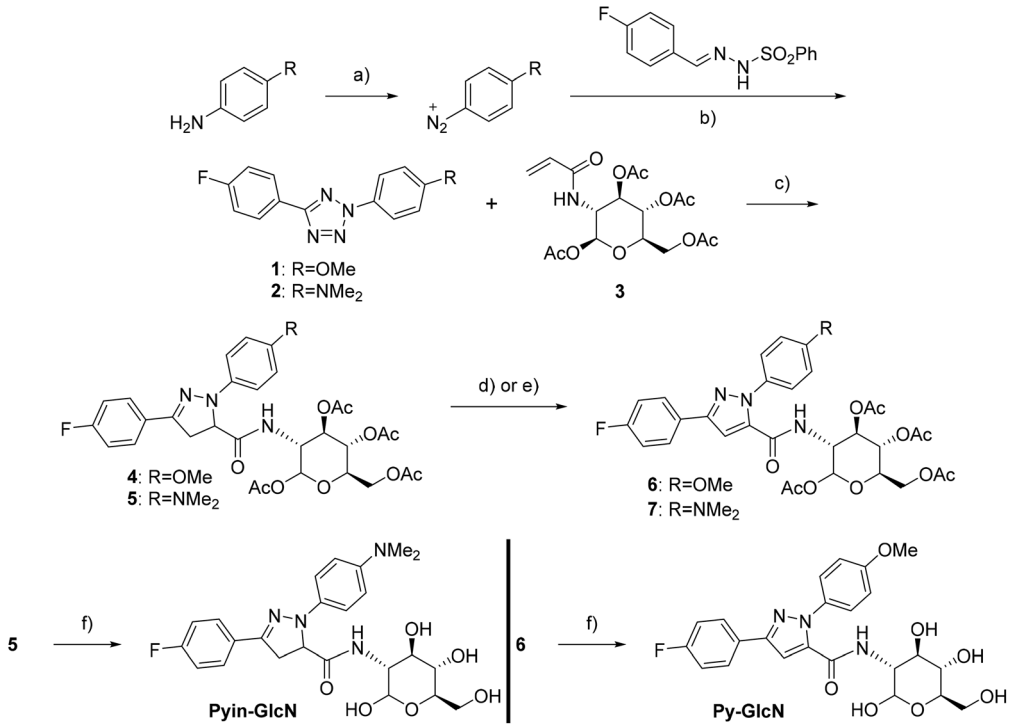

Scheme 1 Synthesis of **Py-GlcN** and **Pyin-GlcN**: (a) $NaNO_2$, HCl, EtOH, 0 °C, 1 h; (b) pyridine, −15 °C, 1 h, **1**: 44%, **2**: 3% yield; (c) 365 nm light, CH_3CN, 1–3 days, **5**: 89% yield; (d) 365 nm light, CH_3CN, air, **6**: 35% yield; (e) DDQ, CH_2Cl_2, overnight; (f) NaOH, MeOH/H_2O, 10 min, **Pyin-GlcN**: 45%, **Py-GlcN**: 45% yield.

byproduct. When R = Me or *tert*-Bu, the reaction took several days and provided incomplete conversion (yields <5%).

Following the formation of **5** and **6**, a deacetylation reaction was performed using NaOH in aqueous methanol. **Py-GlcN** and **Pyin-GlcN** could be synthesized in decent yields (both 45% yield). The yields of the final hydrolysis reaction were lower than expected likely due to loss during HPLC purification. Attempts to obtain the pyrazoline fluorophore of **Py-GlcN** failed as the compound readily oxidized to the respective pyrazole under the reaction conditions. Oxidation of compound **5** with DDQ in CH_2Cl_2 resulted in a non-fluorescent pyrazole **7**. Hence, only pyrazoline **Pyin-GlcN** was used for further evaluation. **Pyin-GlcN** could be isolated and stored as it was more stable against oxidation than **Py-GlcN**. The synthesis of probes **CO-GlcN-1** and **CO-GlcN-2** as coumarin-based fluorophores conjugated to glucosamine is depicted in Scheme 2.

The fluorescence of coumarin **7** is quenched due to the presence of the azide group, a phenomenon previously described by Sivakumar *et al.* in similar coumarin derivatives.[28] A Cu-catalyzed azide–alkyne click reaction was used to couple alkyne **8** to azide **7** to create fluorescent triazole-linked compound **9**.[28,29] The reaction proceeded with 68% yield. However, the following deprotection step proved to be a substantial challenge. Several reaction conditions were tested to remove the acetyl protecting groups, but none gave a satisfactory yield. Using very mild deprotection conditions, stirring **9** with K_2CO_3 in aqueous MeOH for 30 min provided **CO-GlcN-1** in only 6% yield, leaving mostly partially deprotected products.

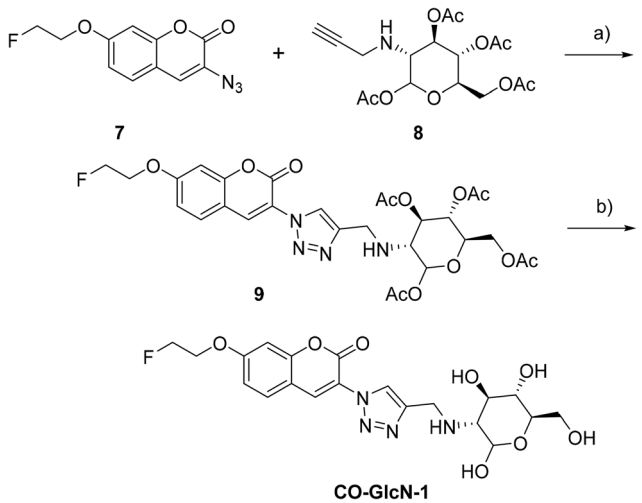

Scheme 2 Synthesis of **CO-GlcN-1**: (a) $CuSO_4{\cdot}5H_2O$, NaAsc, *t*-BuOH, H_2O, acetone, 24 h, 68% yield; (b) K_2CO_3, MeOH/H_2O, 30 min, 6% yield.

When the deprotection reaction with K_2CO_3 in aqueous MeOH was left overnight, there were several uncharacterized degradation products, none of which corresponded to the desired compound.

Upon reacting compound **9** under basic conditions with LiOH in THF/H_2O, or NaOH in MeOH/H_2O, interestingly, amine **10** was formed (Scheme 3). Deprotection with HCl and heat also did not yield the desired product.

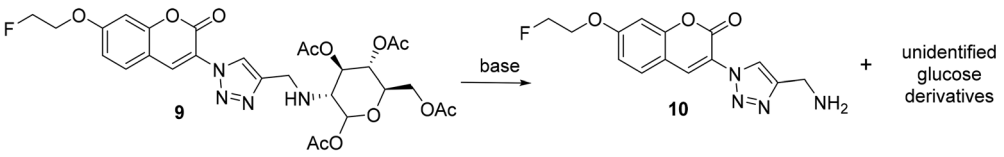

Scheme 3 Side reaction from acetyl deprotection under basic conditions.

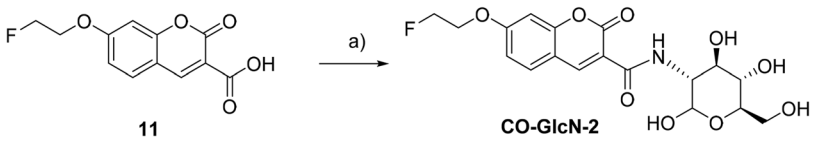

Scheme 4 Synthesis of **CO-GlcN-2**: (a) glucosamine·HCl, HBTU, DIPEA, DMF, overnight, 74% yield.

Probe **CO-GlcN-2** was prepared *via* a simple amide-coupling reaction between carboxylic acid **11** and glucosamine. This HBTU mediated reaction provided **CO-GlcN-2** in 74% yield after HPLC purification (Scheme 4).

Inspired by the favourable properties of GLUT1-selective fluorescent glucose compound 2-NBDG, we set up the synthesis of a respective fluorine-containing analog. Starting from commercially available precursor **12**, an electrophilic aromatic substitution with chlorosulfonic acid afforded sulfonyl chloride **CBDF** in 86% yield.[30] Next, a halogen exchange was performed on **CBDF** with KHF_2 to give **FBDF** in quantitative yield using a modified procedure by Dong *et al.*[31] Finally, **FBDF** underwent a nucleophilic aromatic substitution reaction with glucosamine to furnish **2-FBDG** in 99% yield. This rapid synthetic route led to a compound with extremely desirable optical properties (Table 1) in 85% overall yield over three steps. The synthesis of **2-FBDG** is depicted in Scheme 5.

The original synthetic route towards a benzoxadiazole-fluorophore involved the formation of a sulfonamide from **CBDF** using an amine. However, the addition of glucosamine to **CBDF** produced only **2-FBDG**. The fluoride anion liberated from the S_NAr reaction reacted with the sulfonyl chloride to form the thermodynamically more stable sulfonyl fluoride. Therefore, step (b) of Scheme 5 was not required, but for the sake of unambiguous product identity, the halogen exchange was performed. Additionally, synthesis of **FBDF** was necessary because it was used for identification purposes as a non-radioactive reference compound for radiochemistry. The spectral properties of non-radioactive dual-probes are summarized in Table 1.

Table 1 Fluorescent properties of GlcN-based dual-probes under aqueous conditions (pH 7.4)

Compound	λ (excitation)	λ (emission)
Py-GlcN	320	440
Pyin-GlcN	320	450
CO-GlcN-1	340	420
CO-GlcN-2	350	400
2-FBDG	425	570

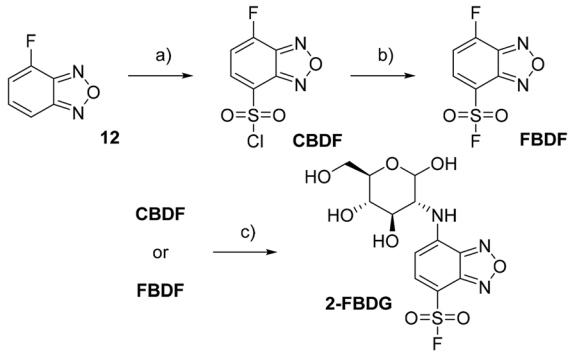

Scheme 5 Synthesis of **2-FBDG**: (a) HSO_3Cl, $CHCl_3$, 0 °C – reflux, 3 h, 86% yield; (b) KHF_2, CH_3CN, H_2O, rt, 2 h, 99% yield; (c) glucosamine, $NaHCO_3$, DMF, rt, overnight, 99% yield.

The pyrazole/pyrazoline and coumarin fluorophores absorb in the UV region and fluoresce between 400–450 nm. The slight hypsochromic shift in emission wavelength and smaller Stokes shift of **CO-GlcN-2** as compared to **CO-GlcN-1** is likely due to the lack of the triazolyl linker.

2-FBDG absorbs in the visible region and fluoresces at a wide range of wavelengths with a peak at 570 nm, which is more red-shifted than 2-NBDG (Fig. 2).

In vitro competition against uptake of 2-[^{18}F]FDG

All novel dual-probes were used in an *in vitro* competition assay to test their interaction with GLUT1. **2-[^{18}F]FDG** was used as the known GLUT1-selective radiotracer assay, which was recently developed by our research group.[32] The murine mammary carcinoma cell line EMT6 used in this assay is known to express high levels of GLUT1.[32,33]

Fig. 3 summarizes the effects of increasing concentrations of all five novel dual-probes, as well as reference compounds D-glucose and 2-NBDG – both of which are known to be transported by GLUT1. Fig. 3 also contains the calculated half-maximum inhibitory concentrations (IC_{50}) for each analyzed compound. Dual-probes **Py-GlcN**, **Pyin-GlcN**, **CO-GlcN-2**, and **2-FBDG** all showed substantial inhibition of **2-[^{18}F]FDG** uptake

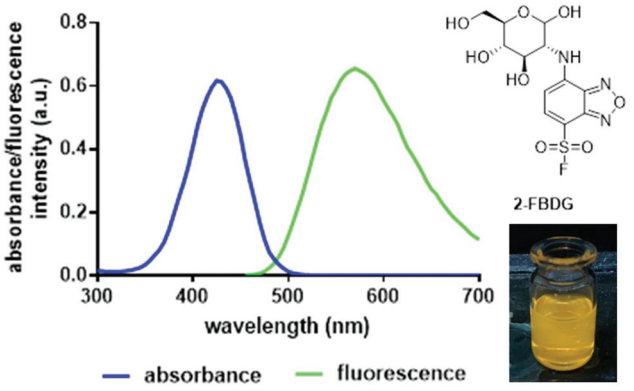

Fig. 2 Absorbance and fluorescence spectra of **2-FBDG** in pH 7.4 Krebs–Ringer buffer. Bottom right shows an image of the solution irradiated at 365 nm using a UV lamp.

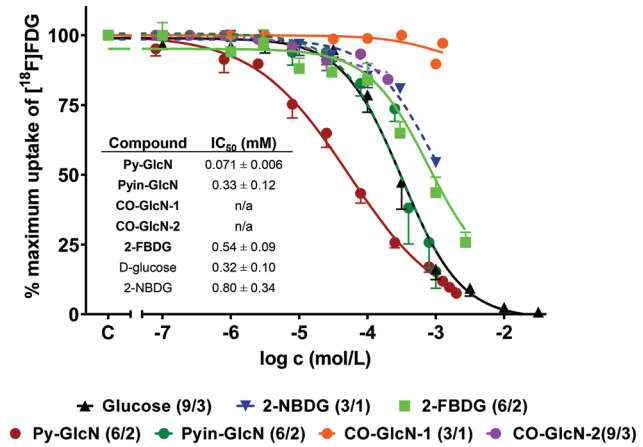

Fig. 3 Inhibition of **2-[^{18}F]FDG** uptake into EMT6 cells using increasing concentrations of test dual-probes in comparison to reference compounds D-glucose and 2-NBDG. Data shown as mean ± SEM from *n* data points out of *x* experiments. Calculated IC_{50} values for **2-[^{18}F]FDG** uptake inhibition are shown in the table of Fig. 3.

into EMT6 cells. **CO-GlcN-1** did not show any effect even at a high concentration of 1 mM. Among all compounds tested, **Py-GlcN** exhibited the highest potency (IC_{50} of 71 ± 6 μM; *n* = 6/2), providing evidence that **Py-GlcN** is better recognized by GLUT1 than its natural substrate D-glucose. Compound **Pyin-GlcN** resulted in a similar potency to D-glucose (IC_{50} of 330 ± 120 μM; *n* = 6/2 *vs.* 320 ± 100 μM; *n* = 9/3). Compound **CO-GlcN-2** only showed a trend for similar inhibition as 2-NBDG, but analysis of higher concentrations was impossible due to its limited solubility. **2-FBDG** had a potency between D-glucose and 2-NBDG (IC_{50} of 540 ± 9 μM; *n* = 6/2). The good potency of compound **2-FBDG** combined with the opportunity to introduce [^{18}F]fluoride make **2-FBDG** an interesting candidate for radiolabeling and further analysis, including PET imaging. While the other potential dual-probes could easily be fluorinated by S_NAr or S_N2 chemistry of their appropriate precursors, **2-FBDG** was also the only probe that possessed both emission and excitation wavelengths in the visible region, rendering it more biocompatible than the other candidates. Another advantage is that the Cl–^{18}F halogen exchange is operationally simpler than the substitution methods noted above as it obviates the need for a fluoride-drying step.

Recent work from Brito *et al.* showed that certain aromatic *N*-glucosides could form a nanoscale supramolecular network around cancer cells expressing GLUT1.[34] They reported that the sterically large *N*-fluorenylmethyloxycarbonyl-glucosamine-6-phosphate is recognized by GLUT1 but is not transported. Instead, the fluorenyl moiety forms π-stacking interactions with other fluorenyl groups to form a barrier-like structure around cells. This effect could potentially explain why **Py-GlcN** was one order of magnitude more potent than glucose itself, assuming the diarylpyrazole moiety mimics a fluorenyl group as in *N*-fluorenylmethyloxycarbonyl-glucosamine-6-phosphate.

Confocal microscopy experiments

To further analyze and confirm that **2-FBDG** is being transported and taken up into the cells *via* GLUT1 instead of being only membrane-bound, qualitative confocal microscopy experiments were performed using breast cancer cell lines EMT6 (murine) and MDA-MB231 (triple-negative human breast cancer cell line) to visualize intracellular localization of **2-FBDG.**

As shown in Fig. 4, there is evident cytosolic uptake of compound **2-FBDG.** Additionally, intracellular uptake of **2-FBDG** was inhibited in the presence of extracellular high levels of D-glucose, providing further evidence that **2-FBDG** is transported by GLUT1 and results in intracellular uptake in murine and human breast cancer cells.

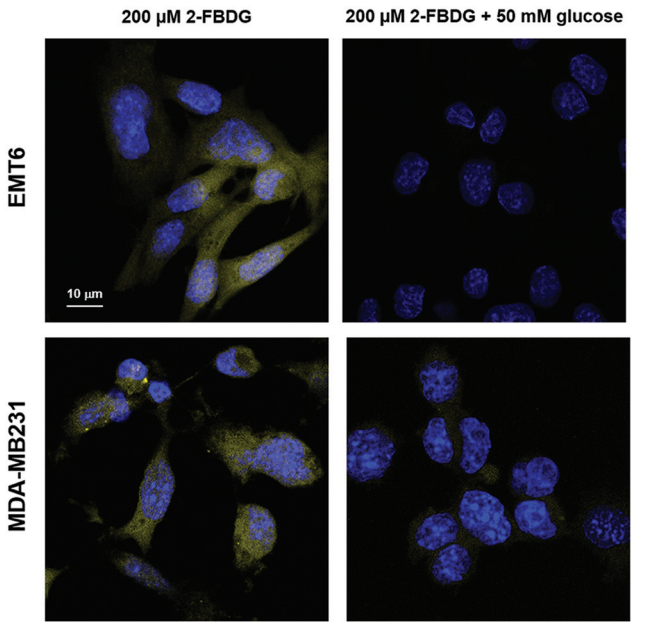

Fig. 4 Confocal microscopy images were obtained in two different breast cancer cell lines: EMT6 and MDA-MB-231. The cells were incubated with 200 μM of **2-FBDG** in the absence or presence of 50 mM glucose for 1 h. DAPI was used as a nuclear stain.

Radiochemistry

The radiosynthesis of **2-[^{18}F]FBDG** was accomplished *via* prosthetic group **[^{18}F]FBDF** and subsequent S_NAr reaction with glucosamine (Scheme 6).

[^{18}F]FBDF was formed by applying mild sulfonyl [^{18}F]fluoride chemistry, employing aqueous conditions and room temperature, which was introduced by Inkster *et al.*[35] Briefly, aqueous no-carrier-added (n.c.a) [^{18}F]CsF was added to a solution of sulfonyl chloride **17** in *tert*-BuOH, followed by the addition of pyridine and subsequent incubation at room temperature for 15 min. After several attempts, it became evident that pyridine was degrading prosthetic group **[^{18}F]FBDF**. The rationale for adding pyridine was that it scavenges unreacted sulfonyl chloride to simplify purification and yields radiolabeled compounds at high molar activity.[35] However, in our case, the need for this step is negligible as a high molar activity is not a concern for the radiotracer due to ubiquitous glucose present in the blood. Additionally, the subsequent S_NAr reaction generates a free fluoride anion which reacts with the sulfonyl chloride. This consumes the remaining sulfonyl chloride and ensures high chemical purity.

Following these findings, the addition of pyridine was omitted, and the formation of **[^{18}F]FBDF** was achieved in nearly quantitative yields. The fluorination reaction was usually complete within 5 minutes.

For further radiosynthesis optimization, some different precursor concentrations were also tested, showing that as little as 100–200 μg of precursor **CBDF** in 200 μL *tert*-BuOH provided consistent quantitative yields within a 5 min reaction time. Lowering the amount of labelling precursor **CBDF** to 20 μg still resulted in a 70% ^{18}F incorporation within 15 min.

Following the radiofluorination step, **[^{18}F]FBDF** was trapped on a solid-phase cartridge and eluted with DMF into a vial containing glucosamine and $NaHCO_3$ to start the S_NAr reaction. Several different cartridges were tested (Waters Sep-Pak tC18 Plus Light, Waters Sep-Pak tC18 Plus, and Macherey-Nagel Chromafix C18), but they either had low trapping efficiency or required too much DMF to elute the product. We found that directly diluting the initial reaction mixture with 600 μL DMF and omitting the solid-phase extraction had no detrimental effect on the S_NAr reaction. This procedure simplified the synthetic sequence and vastly improved the final decay-corrected radiochemical yield after HPLC from 20% to 69 ± 3% (n = 3) over two steps in <110 min total synthesis time, including isolation and reformulation in saline for subsequent *in vivo* studies. When starting with 200 μg of **CBDF** and 234 MBq of [^{18}F]CsF, the effective molar activity achieved was 96 MBq μmol^{-1}. The effective molar activity can be improved by increasing the amount of starting radioactivity and by lowering the amount of compound **17**. This reaction is also advantageous because of the short reaction times and the absence of a fluoride drying step.

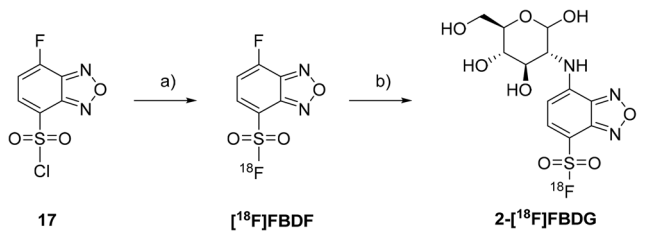

Scheme 6 Radiolabeling of **2-FBDG**: (a) [^{18}F]CsF, H_2O, *tert*-BuOH, rt, 5 min; (b) glucosamine·HCl, $NaHCO_3$, DMF, H_2O, *t*-BuOH, rt, 20 min.

Animal experiments

Dual-probe **2-[^{18}F]FBDG** was evaluated *in vivo* with PET imaging experiments in NIH-III mice bearing MDA-MB231 breast cancer xenografts. PET images were collected dynamically over 60 min after the injection of radiotracer **2-[^{18}F]FBDG** (~5 MBq in saline) into the tail vein.

Fig. 5 summarizes the PET images at selected time points compared to **2-[^{18}F]FDG** in the same mouse. While uptake into MDA-MB-231 tumours increased after injection of **2-[^{18}F]FDG** over time, this was not observed with **2-[^{18}F]FBDG**. Instead, bone uptake increased over time while background clearance in reference muscle tissue was detected. Fig. 6 depicts the kinetic profile of **2-[^{18}F]FBDG** accumulation and clearance in MDA-MB231 tumours, muscle and bone as analyzed from respective time-activity curves (TACs) over time. Interestingly, some radioactivity was delivered to the MDA-MB231 tumours and was selectively trapped as no washout was observed compared to muscle as reference tissue.

The bone TAC showed that after reaching an initial low-level uptake at 5 min, a systematic and continuous increase in bone uptake was observed over time. When compared with a [^{18}F]NaF injection, the bone uptake of **2-[^{18}F]FBDG** followed a similar trend over time, but on a lower level. The latter indicates a metabolic change of **2-[^{18}F]FBDG** *in vivo* represented by a radiodefluorination process.[36] To confirm this observation, further analysis of the radiotracer's stability was carried out by examining mouse blood samples over time.

Metabolic stability of **2-[^{18}F]FBDG** was assessed in a normal mouse by analyzing blood samples at 5, 15, 30, and 60 minutes p.i. The blood samples were centrifuged to remove the blood cells, and the resulting supernatant was treated with methanol to precipitate the proteins. Second centrifugation followed by HPLC analysis of the remaining supernatant provided data on the plasma's free radiotracer content. The graph shown in Fig. 7 represents the amounts of intact **2-[^{18}F]FBDG** *versus* **[^{18}F]F$^-$** as radiometabolite over the time course of 60 min.

However, the metabolic stability of **2-[^{18}F]FBDG** may be even lower as constant bone uptake of free **[^{18}F]F$^-$** occured over time, removing it from the blood and plasma.

The extraction efficiency (the amount of radioactivity recovered) was quite low, which further exemplifies this hypothesis. This is consistent with the uptake profile in the tumor-bearing mice where bone uptake was also detected (Fig. 5 and 6). Also, the full extent of radiodefluorination could potentially be underestimated as it has been shown that **[^{18}F]F$^-$** can retain on reverse-phase silica columns (especially when using solvents with pH < 5), and therefore not be detected by the radio-

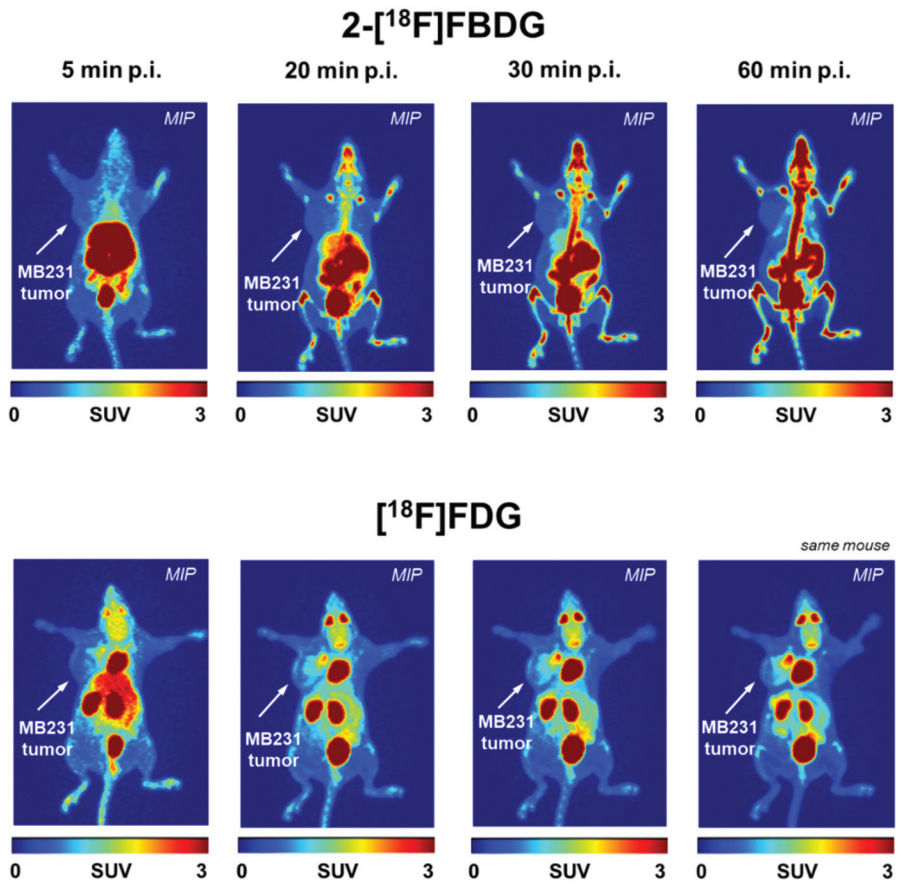

Fig. 5 Uptake of **2-[^{18}F]FBDG** (top) and **2-[^{18}F]FDG** (bottom) in a MDA-MB231 tumor-bearing mouse taken at 5, 20, 30, and 60 min (p.i. = post-injection, SUV = standardized uptake value).

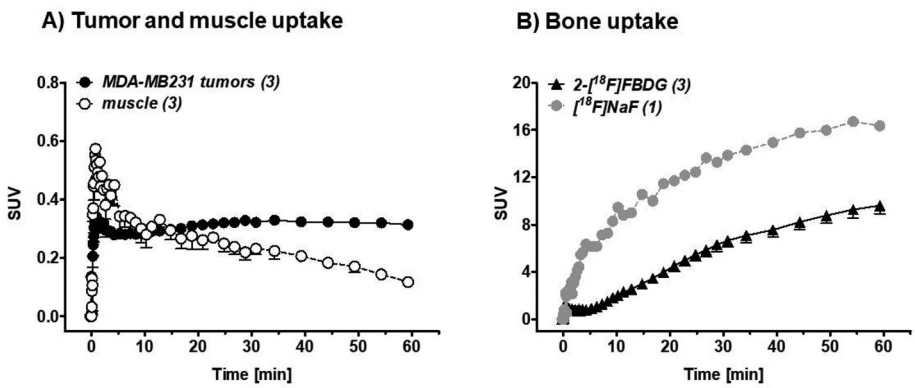

Fig. 6 Time-activity curves (TACs) of **2-[^{18}F]FBDG** *in vivo*. A: Comparison of SUV between MDA-MB231 tumours and muscle; B: comparison of SUV in the bone between injection of **2-[^{18}F]FBDG** *versus* injection of **[^{18}F]NaF**.

detector.[37] To mitigate this, we used acid-free distilled water in our mobile phase. In addition, the stability of **2-[^{18}F]FBDG** was evaluated *in vitro* in saline, and 4% free **[^{18}F]F$^-$** was observed after 10 min (time = 0 min in Fig. 7), increasing to 8% free **[^{18}F]F$^-$** after 4.5 hours. This was indicative of the greater benchtop chemical stability of the radiotracer compared to the *in vivo* stability.

The present results are consistent with recent literature concerning the stability of sulfonyl [^{18}F]fluorides.[35,38,39] Sulfonyl fluorides are known to act as 'privileged warheads' and react with protein-based nucleophiles under special conditions.[40] The release of free [^{18}F]fluoride from radiotracer **2-[^{18}F]FBDG** can also be explained by nucleophilic attacks on the sulfonyl [^{18}F]fluoride *in vivo* by plasma proteins.

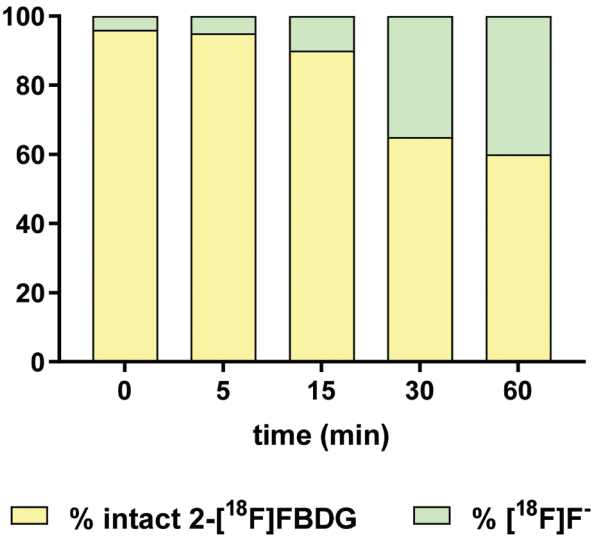

Fig. 7 Metabolic stability of 2-[^{18}F]FBDG *in vivo*. Blood samples were taken at 5, 15, 30, and 60 min, processed and subjected to analytical radio-HPLC analysis to determine the amounts of intact 2-[^{18}F]FBDG.

Additionally, the S–F bond of sulfonyl fluorides have been shown to be more stable as steric bulk increases.[39] This characteristic is also described in the well established [^{18}F]SiFA motif, where the Si–F bond benefits from steric bulk around the respective functional group to protect against radiodefluorination.[41] The electronic nature of the benzoxadiazole ring may also be contributing to the instability of the sulfonyl fluoride. We first postulated that the electron-rich aromatic system would discourage nucleophilic attack and/or hydrolysis of the sulfonyl fluoride. While **2-[^{18}F]FBDG** did exhibit stability to water, the *in vivo* stability was not satisfactory. Analagous to [^{18}F]sulfonyl fluorides, [^{18}F]trifluoroaryl borates also initially suffered from radiodefluorination *in vivo* before it was found that *ortho* electron-withdrawing groups stabilize the B–F bond.[42] Interestingly, it was shown that radiolabeled aryl [^{18}F] fluorosulfates were more stable than sulfonyl fluorides, and no radiodefluorination was observed *in vivo*.[43] Indeed, the stability of these S–F bonds vary greatly, and further investigation into the stereoelectronic effects governing the stability of the S–F bond in sulfonyl fluorides could produce more promising iterations of **2-[^{18}F]FBDG**.

Conclusion

In this study, we have introduced various synthesis pathways for the preparation of different glucose-based dual PET/Fl imaging probes for targeting facilitated hexose transporter GLUT1. Compound **2-FBDG** shows excellent potential as an *in vitro* fluorescent probe with retained affinity to GLUT1. Dual-probe **2-[^{18}F]FBDG** interacts with GLUT1 and is transported by GLUT1 into murine and human breast cancer cells. Further research is required to address its *in vivo* metabolic stability concerns to improve the radiotracer's tumor uptake and clearance profile. This work may include fluorophores with more stable C–F bonds, or the relatively new and mostly unexplored pentafluorosulfanyl group.[38]

Experimental

Chemistry

General methods. All reagents were purchased from commercial sources and used without further purification. NMR spectra were recorded using the Agilent DD2 400, Varian Inova 500, Varian VNMRS 500, Varian VNMRS 600, Bruker Avance III 600, or the Agilent VNMRS 700. ^{1}H and ^{13}C NMR spectra were referenced to the residual signals of deuterated solvents as internal standards. Coupling constants (J) are reported in hertz (Hz). Low resolution mass spectra were acquired using an Agilent 6130 Mass Spectrometer coupled with an Agilent 1260 HPLC instrument. High resolution mass spectra were acquired using the Agilent Technologies 6220 oaTOF (ESI) or the Kratos MS50G (EI). Absorbance and fluorescence spectra were acquired using a BioTek Synergy H1 Multi Detection Microplate Reader. Column chromatography was performed using 230–400 mesh silica gel. TLC analyses were completed on silica gel 60 F_{254} aluminum plates, purchased from Millipore-Sigma. Photo-click reactions were performed using a tabletop TLC UV lamp (23 W). Semi-preparative HPLC was performed on a Gilson system (Mandel Scientific, Guelph, ON, Canada) with a 321 pump and a 155 dual-wavelength detector (using 210 and 254 nm) installed with a Phenomenex Jupiter 10u Proteo 90 Å, 250 × 10 mm, 4.5 μm C12 column. Analytical HPLC was performed on a Shimadzu system (Mandel Scientific, Guelph, ON, Canada) equipped with a DGU-20A5 degasser, a SIL-20A HT autosampler, a LC-20AT pump, a SPD-M20A photodiodearray detector, and a Ramona Raytest radiodetector using a Phenomenex Luna 10u C18(2) 100A, 250 × 4.6 mm column.

5-(4-Fluorophenyl)-2-(4-methoxyphenyl)-2*H*-tetrazole (1). The tetrazole was synthesized according to a published procedure,[44] purified using flash column chromatography (10 : 1 hexanes/EtOAc), and two recrystallization steps (hexanes/EtOAc) – this produced a white solid 430 mg, 1.59 mmol, 44% yield. R_f (10 : 1 hexane/EtOAc) = 0.32; **mp** = 139 °C; **^{1}H NMR** (600.27 MHz, $CDCl_3$) δ 3.90 (s, 3 H), 7.06/8.09 (AA′BB′, 4 H), 7.21/8.23 (AA′BB′, 4 H); **^{13}C NMR** (150.94 MHz, $CDCl_3$) δ 55.6, 114.7, 116.1 (d, $^{2}J_{C-F}$ = 22.1 Hz), 121.4, 123.5 (d, $^{4}J_{C-F}$ = 3.3 Hz), 129.0 (d, $^{3}J_{C-F}$ = 8.3 Hz), 130.4, 160.5, 164.1 (d, $^{1}J_{C-F}$ = 250.0 Hz), 164.9; **^{19}F NMR** (564.82 MHz, $CDCl_3$) δ −109.82 (tt); **LRMS** (ESI) m/z: $[M + H]^+$ calcd for $C_{14}H_{12}FN_4O$ 271.1: found 271.1; **UV/Vis** (CH_3CN): absorbance λ_{max} (ε): 290 nm (18 800 L mol^{-1} cm^{-1}), 275 nm (18 300 L mol^{-1} cm^{-1}).

1,3,4,6-Tetra-*O*-acetyl-2-acrylamido-2-deoxy-D-glucose (3). The product was synthesized according to a published procedure.[45] The crude reaction mixture was concentrated, then purified by flash column chromatography using a gradient of 50% EtOAc/hexanes to 75% EtOAc/hexanes. A pure white powder was obtained, 158 mg, 0.393 mmol, 99% yield. R_f (1 : 1 EtOAc/

hexanes) = 0.26; **^{1}H NMR** (600.27 MHz, $CDCl_3$) δ 2.02 (s, 3 H), 2.04 (s, 3 H), 2.1 (d, J = 1.9 Hz, 6 H), 3.83 (m, 1 H), 4.14 (dd, J = 2.3, 12.6 Hz, 1 H), 4.28 (dd, J = 4.7, 12.4 Hz, 1 H), 4.41 (m, 1 H), 5.17 (m, 2 H), 5.70 (m, 3 H), 6.01 (dd, J = 10.4, 16.9 Hz, 1 H), 6.25 (d, J = 16.6 Hz, 1 H); **^{13}C NMR** (150.94 MHz, $CDCl_3$) δ 20.58, 20.59, 20.7, 20.8, 53.0, 61.6, 67.6, 72.5, 73.1, 92.7, 127.8, 130.0, 165.4, 169.2, 169.6, 170.7, 171.3. **LRMS** (ESI) m/z: $[M + Cl^-]^-$ calcd for $C_{17}H_{23}ClNO_{10}$ 436.1: found 436.1.

Compound 6. Tetrazole **1** (0.136 mmol) and **3** (0.177 mmol) were dissolved in acetonitrile. This solution was irradiated at 365 nm for several days. The pyrazoline **4** oxidizes to the pyrazole under ambient conditions over the course of the reaction. The acetonitrile was removed under reduced pressure, and the resulting solids were purified by flash column chromatography (30% EtOAc/hexanes to 50% EtOAc/hexanes). A white solid was isolated, 30.6 mg, 0.0477 mmol, 34.7% yield. R_f (1 : 1 EtOAc/hexanes) = 0.45; **^{1}H NMR** (600.27 MHz, $CDCl_3$) δ 2.03 (s, 3 H), 2.06 (s, 3 H), 2.10 (d, 6 H), 3.81 (m, 1 H), 3.86 (s, 3 H), 4.14 (dd, J = 2.3, 12.5 Hz, 1 H), 4.27 (dd, J = 4.6, 12.5 Hz, 1 H), 4.35 (m, 1 H), 5.16 (m, 2 H), 5.71 (d, 1 H), 6.04 (d, J = 8.8 Hz, 1 H), 6.91 (s, 1 H), 7.37/6.97 (AA′BB′, 4 H), 7.81/7.12 (AA′BB′, 4 H); **^{13}C NMR** (150.94 MHz, CD_3Cl) δ 20.56, 20.63, 20.69, 20.84, 53.3, 55.6, 61.6, 67.5, 72.3, 73.0, 92.5, 105.5, 114.1, 115.7 (d, $^2J_{C-F}$ = 22.1 Hz), 126.8, 127.5 (d, $^3J_{C-F}$ = 7.7 Hz), 128.27 (d, $^4J_{C-F}$ = 3.2 Hz), 132.7, 137.3, 150.4, 159.0, 159.8, 162.9 (d, $^1J_{C-F}$ = 247.7 Hz), 169.2, 169.3, 170.1, 171.2; **LRMS** (ESI) m/z: $[M + H]^+$ calcd for $C_{31}H_{33}FN_3O_{11}$ 642.2: found 642.2.

Py-GlcN. Compound **6** (0.027 mmol) was dissolved in MeOH (4 mL) and 0.125 M NaOH (1 mL). The solution was stirred at room temperature for 10 minutes. The solution was then neutralized with 1 M HCl. Excess solvent was removed under reduced pressure. The resulting solids were purified by reverse-phase HPLC using a flow rate of 2 mL min^{-1} with the following gradient where H_2O (0.2% TFA) is solvent A and CH_3CN is solvent B: 0–5 min 20% B, 10 min 35% B, 20 min 50% B, 32 min 84% B, then lyophilized. A white solid was recovered, 5.7 mg, 0.012 mmol, 45% yield. **^{1}H NMR** (498.12 MHz, CD_3OD) δ 3.31–3.95 (m, 9 H), 4.70 (d, β-anomer proton, J = 8.3 Hz), 5.16 (d, α-anomer proton, J = 3.5 Hz), 7.20 (s, 1 H), 7.00/7.47 (AA′BB′, 4 H), 7.15/7.87 (AA′BB′, 4 H); **^{13}C NMR** (125.69 MHz, CD_3OD) mixture of α/β anomers δ 56.02, 56.05, 56.3, 59.0, 62.8, 62.9, 72.3, 72.5, 72.6, 73.2, 75.9, 78.2, 92.4, 96.9, 106.4, 106.8, 115.0, 115.1, 116.6 (d, $^2J_{C-F}$ = 21.6 Hz), 127.0, 127.3, 128.74 (d, $^3J_{C-F}$ = 8.2 Hz), 128.77 (d, $^3J_{C-F}$ = 8.2 Hz), 130.17, 130.20, 134.40, 134.46, 139.96, 140.03, 151.64, 151.68, 162.0 (d, $^1J_{C-F}$ = 245.9 Hz), 161.1, 163.0, 164.3 (d, $^1J_{C-F}$ = 245.9 Hz); **^{19}F NMR** (468.64 MHz, CD_3OD) −77.04 (s, TFA), −115.88 (m); **HRMS** (ESI) m/z: $[M + Na]^+$ calcd for $C_{23}H_{24}FN_3O_7Na$ 496.1490: found 496.1494; **UV/Vis** (1 : 1 [CH_3CN] : [pH 7.4 PBS]): absorbance λ_{max} (ε): 230 nm (7900 L mol^{-1} cm^{-1}); fluorescence (1 : 1 [CH_3CN] : [pH 7.4 PBS]): λ_{max} = 440 nm (320 nm excitation).

4-(5-(4-Fluorophenyl)-2*H*-tetrazol-2-yl)-*N*,*N*-dimethylaniline (2). The tetrazole was synthesized according to a published procedure with slight modifications.[44] Instead of quenching the pyridine with HCl, the reaction mixture was washed with NaOH, extracted with CH_2Cl_2, and concentrated under vacuum. The crude compound was purified using a silica gel column (with 10 : 1 hexane/EtOAc) and a recrystallization step (hexanes/toluene) – this produced yellow crystals, 110 mg, 0.39 mmol, 3% yield. R_f (10 : 1 hexanes/EtOAc) = 0.27; **^{1}H NMR** (600.27 MHz, $CDCl_3$) δ 3.74 (s, 6 H), 6.81/8.01 (AA′BB′, 4 H), 7.21/8.24 (AA′BB′, 4 H); **^{13}C NMR** (150.94 MHz, $CDCl_3$) δ 40.4, 111.9, 116.0 (d, $^2J_{C-F}$ = 22.1 Hz), 121.1, 123.9 (d, $^4J_{C-F}$ = 3.3 Hz), 126.6, 128.9 (d, $^3J_{C-F}$ = 7.7 Hz), 151.1, 163.8, 164.0 (d, $^1J_{C-F}$ = 249.9 Hz); **^{19}F NMR** (564.82 MHz, $CDCl_3$) δ −110.28 (tt); **LRMS** (ESI) m/z: $[M + H]^+$ calcd for $C_{15}H_{15}FN_5$ 284.1: found 284.2; **UV/Vis** (CH_3CN): absorbance λ_{max} (ε): 330 nm (22 000 L mol^{-1} cm^{-1}), 230 nm (19 000 L mol^{-1} cm^{-1}).

Compound 5. Tetrazole **2** (0.0688 mmol) and **3** (0.0977 mmol) were dissolved in acetonitrile. This solution was irradiated at 365 nm for 3 days. The acetonitrile was removed under reduced pressure, and the resulting solids were purified by flash chromatography (50% EtOAc/hexanes to 66% EtOAc/hexanes). A yellow-green solid was isolated, 35.4 mg, 0.054 mmol, 89% yield. R_f (1 : 1 EtOAc/hexanes) = 0.18; **^{1}H NMR** (600.27 MHz, $(CD_3)_2CO$) δ 1.96–2.03 (d, 12 H), 2.85 (s, 6 H), 3.12 (dq, 1 H), 3.77–4.65 (m, 9 H), 5.03 (dt, 2 H), 5.36 (dt, 1 H), 5.48 (m, 1 H), 5.59 (m, 1 H), 5.92 (ddd, 1 H), 6.07 (dd, 0.5 H), 6.15 (s, 0.5 H), 6.16 (d, 0.5 H), 6.75/6.94 (AA′BB′, 4 H), 7.20/7.98 (AA′BB′, 4 H) [contains additional signals due to epimers and oxidized product]; **^{13}C NMR** (150.94 MHz, $(CD_3)_2CO$) δ 20.62, 20.68 (t), 20.8 (d, J = 11.9 Hz), 20.9 (d, J = 3.9 Hz), 40.0 (d, J = 17.7 Hz), 41.6 (d, J = 4.2 Hz), 53.7 (d, J = 5.8 Hz), 54.1, 62.6 (d, J = 3.9 Hz), 67.0 (d, J = 11.3 Hz), 69.4 (d, J = 3.0 Hz), 69.6, 72.4, 73.4 (m), 92.7, 92.9, 93.1, 115.1 (d, J = 10.0 Hz), 115.7 (d, J = 11.6 Hz), 116.4 (dd, $^2J_{C-F}$ = 21.8 Hz), 126.5, 128.8 (dd, $^3J_{C-F}$ = 8.3 Hz), 130.0 (d, J = 3.0 Hz), 132.1, 138.7 (d, J = 3.6 Hz), 147.0 (d, J = 7.5 Hz), 163.9 (dd, $^1J_{C-F}$ = 247.4 Hz), 169.4, 169.5, 170.1, 170.4, 170.6, 170.7, 170.8 (d, J = 3.0 Hz), 172.7, 172.9 [mixture of epimers and oxidized product]; **LRMS** (ESI) m/z: $[M + H]^+$ calcd for $C_{32}H_{38}FN_4O_{10}$ 657.3: found 657.2.

Pyin-GlcN. Compound **5** (0.046 mmol) was dissolved in MeOH (4 mL) and 0.120 M NaOH (1 mL). The solution was stirred at room temperature for 10 minutes. The solution was then neutralized with 1 M HCl. Excess solvent was removed under reduced pressure. The resulting solids were purified by reverse-phase HPLC using a flow rate of 2 mL min^{-1} with the following gradient where H_2O (0.2% TFA) is solvent A and CH_3CN is solvent B: 0–5 min 20% B, 10 min 35% B, 20 min 50% B, 32 min 84% B, then lyophilized. A pale colorless solid was recovered, 10.7 mg, 0.022 mmol, 45% yield. **^{1}H NMR** (600.27 MHz, HDO + H_2O suppression) δ 3.22/3.32 (s, 6 H), 3.36–3.90 (m, 6 H), 4.64 (d, J = 8.4 Hz, 1 H), 4.89 (m, 2 H), 5.16 (α-anomeric proton, d, J = 3.6 Hz, 1 H), 7.15 (m, 4 H), 7.46 (m, 2 H), 7.73 (m, 2 H); **^{13}C NMR** (150.94 MHz, D_2O) δ 39.2, 46.4, 54.1/54.2, 56.6, 60.5/60.6, 63.16/62.50, 70.0, 70.2, 70.5, 71.51/71.56, 73.43/73.59, 75.9, 90.7, 94.7, 113.8, 115.8 (d, $^2J_{C-F}$ = 21.8 Hz), 121.3, 121.5, 126.5 (d, J = 7.7 Hz), 127.1, 127.9, 128.3, 133.8, 145.4, 151.2, 163.4 (d, $^1J_{C-F}$ = 245.0 Hz), 173.7 (different protonation states); **LRMS** (ESI) m/z: $[M + H]^+$ calcd for $C_{24}H_{30}FN_4O_5$ 489.2: found 489.2. **UV/Vis** (pH 7.4 PBS): absor-

bance λ_{max} (ε): 250 nm (12 640 L mol^{-1} cm^{-1}), 320 nm (9300 L mol^{-1} cm^{-1}); fluorescence (pH 7.4 PBS): λ_{max} = 450 nm (320 nm excitation).

3-Azido-7-(2-fluoroethoxy)-2*H*-chromen-2-one (7). 3-Azido-7-hydroxy-2*H*-chromen-2-one, which was synthesized according to a published procedure (0.900 mmol),[28] was stirred with K_2CO_3 (1.35 mmol) in dry DMF (4 mL) for 10 min at 50 °C under N_2. Then 1-fluoro-2-iodoethane (1.35 mmol) was added dropwise, and was allowed to react for 1.5 h. The DMF was removed by reduced pressure, and the residue was resuspended in a solution of 1 : 2 EtOH to 6 M HCl. The product precipitated, which was filtered off and washed with water. This provided a fine red powder, 140.3 mg, 0.563 mmol, 63% yield. R_f (50% EtOAc/hexanes) = 0.78; **^{1}H NMR** (600.27 MHz, $(CD_3)_2CO$) δ 4.42 (m, J = 29.4 Hz, 2 H), 4.82 (m, J = 47.8 Hz, 2 H), 7.00 (s, 1 H), 7.01 (m, 1 H), 7.48 (s, 1 H), 7.58 (d, J = 8.9 Hz, 1 H); **^{13}C NMR** (150.94 MHz, $(CD_3)_2CO$) δ 69.0 (d, $^2J_{C-F}$ = 19.6 Hz), 82.8 (d, $^1J_{C-F}$ = 168.5 Hz), 102.1, 114.1, 114.4, 124.1, 127.7, 129.8, 154.1, 158.2, 161.8; **^{19}F NMR** (564.82 MHz, $(CD_3)_2CO$) δ −224.40 (m). **LRMS** (ESI) m/z [M–N_2 + H]$^+$ calcd for $C_{11}H_9FNO_3$ 222.0: found 222.0.

1,3,4,6-Tetra-*O*-acetyl-*N*-(3-trimethylsilyl)propargyl-D-glucosamine. 1,3,4,6-Tetra-*O*-acetyl-β-D-glucosamine hydrochloride (1.0 mmol) and 3-(trimethylsilyl)-2-propynal (1.4 mmol) were dissolved in MeOH (10 mL) and stirred at 40 °C for 30 min, until the solution became clear. $NaCNBH_3$ (1.1 mmol) was added and the solution was stirred overnight at room temperature. The crude reaction mixture was extracted with CH_2Cl_2 then concentrated under vacuum. The crude oil was purified by flash column chromatography (20–50% EtOAc/hexanes) to provide a clear, colorless, viscous oil, 201.3 mg, 0.440 mmol, 44% yield. R_f (1 : 1 EtOAc/hexanes) = 0.61; **^{1}H NMR** (600.27 MHz, $CDCl_3$) δ 0.18 (s, 9 H), 2.04 (s, 3 H), 2.09 (d, J = 5.1 Hz, 6 H), 2.17 (s, 3 H), 3.08 (dd, 1 H), 3.47 (q, 2 H), 3.78 (dq, 1 H), 4.08 (dd, 1 H), 4.30 (dd, 1 H), 5.06 (dt, 2 H), 5.52 (d, J = 8.5 Hz, 1 H); **^{13}C NMR** (150.94 MHz, $CDCl_3$) δ −0.02, 14.2, 20.6, 20.7, 20.9, 21.1, 38.2, 59.4, 60.4, 61.8, 68.2, 72.4, 73.8, 88.0, 95.3, 104.1, 168.9, 169.6, 170.7, 171.1; **LRMS** (ESI) m/z: [M + H]$^+$ calcd for $C_{20}H_{32}NO_9Si$ 458.2: found 458.1.

1,3,4,6-Tetra-*O*-acetyl-*N*-propargyl-D-glucosamine (8). 1,3,4,6-Tetra-*O*-acetyl-*N*-(3-trimethyl-silyl)propargyl-β-D-glucosamine (0.312 mmol) was dissolved in 6 mL dry THF at room temperature and flushed with N_2. TBAF (1 M in THF) was added (0.38 mmol) and the reaction was mixture was stirred for 2 h. The reaction was quenched by adding sat. NH_4Cl and diethyl ether. The product was extracted with diethyl ether, washed with NH_4Cl, water, then brine. The organic layer was concentrated, and the residue was purified by column chromatography (50% EtOAc/hexanes). This provided a pale-yellow oil as a mixture of α/β anomers 73.2 mg, 0.190 mmol, 60% yield. R_f (1 : 1 EtOAc/hexanes) = 0.37/0.44; **^{1}H NMR** (600.27 MHz, $CDCl_3$) δ 2.04 (d, J = 0.75 Hz, 3 H), 2.09 (m, 6 H), 2.18 (d, J = 10.8 Hz, 3 H), 2.23 (dt, 1 H), 3.08 (dd, 0.6 H), 3.20 (dd, 0.4 H), 3.41 (m, 1 H), 3.48 (dt, 1 H), 3.78 (m, 0.6 H), 4.02 (m, 0.4 H), 4.07 (m, 1 H), 4.31 (m, 1 H), 5.02 (dd, 0.6 H), 5.12 (dt, 1 H), 5.21 (dd, 0.4 H), 5.53 (d, J = 0.6 Hz, 8.5 Hz), 6.40 (d, J = 3.6 Hz, 0.4 H); **^{13}C NMR** (150.94 MHz, $CDCl_3$) δ 20.6, 20.72, 20.74, 20.93, 20.95, 20.97, 21.1, 36.8, 37.3, 58.7, 60.0, 61.7, 61.8, 68.1, 68.2, 69.5, 71.4, 72.0, 72.4, 73.8, 90.7, 95.3, 168.98, 169.01, 169.6, 170.7, 171.0, 171.3; **LRMS** (ESI) m/z: [M + H]$^+$ calcd for $C_{17}H_{24}NO_9$ 386.1: found 386.1.

Compound 9. Azide **7** (0.437 mmol) and alkyne **8** (0.428 mmol) were dissolved in a solution of 1 mL *t*-BuOH, 4 mL acetone, and 1 mL water. $CuSO_4 \cdot 5H_2O$ (1.126 mmol) was dissolved in 2 mL water, and sodium ascorbate (5.463 mmol) was dissolved in 4 mL water. The Na-ascorbate solution was added dropwise to the Cu(II) solution. When the solution turned a pale orange colour, 230 μL of this suspension was added to the reaction mixture. The reaction vessel was then flushed with N_2, and the reaction was stirred for 24 h. The reaction mixture was filtered over Celite and washed with 50 mL of acetone. The filtrate was concentrated, and the crude was purified by column chromatography (66% EtOAc/hexanes to 50% EtOAc/40% hexanes/10% acetone to 50% EtOAc/25% hexanes/25% acetone). This provided a pale yellow oil, 185.3 mg, 0.292 mmol, 68% yield. R_f (2 : 1 : 1 EtOAc/hexanes/acetone) = 0.42/0.65 (–OAc); **^{1}H NMR** (600.27 MHz, $CDCl_3$) δ 2.03 (s, 3 H), 2.09 (d, 6 H), 2.21 (s, 3 H), 3.00 (s, 1 H), 3.79 (m, 1 H), 4.08 (m, 1 H), 4.29 (dd, 2 H), 4.33 (m, J = 27.6 Hz, 2 H), 4.83 (m, J = 47.3 Hz, 2 H), 5.07 (dt, 1 H), 5.59 (d, J = 8.5 Hz, 1 H), 6.95 (d, J = 2.4 Hz, 1 H), 7.03 (dd, J = 2.4 Hz, 8.7 Hz, 1 H), 7.60 (d, J = 8.7 Hz, 1 H), 8.51 (d, J = 25.0 Hz, 1 H); **^{13}C NMR** (150.94 MHz, $CDCl_3$) δ 14.2, 20.6, 20.7, 20.9, 21.0, 21.2, 29.7, 42.7, 43.0, 59.8, 60.4, 61.7, 67.7 (d, $^2J_{C-F}$ = 20.5 Hz), 68.2, 72.5, 73.6, 81.3 (d, $^1J_{C-F}$ = 172.2 Hz), 95.1, 101.4, 112.0, 114.3, 122.7, 130.0, 133.4, 154.5, 156.0, 162.4, 169.1, 169.6, 170.7, 171.1; **^{19}F NMR** (564.82 MHz, $CDCl_3$) δ −223.73 (m); **LRMS** (ESI) m/z: [M + H]$^+$ calcd for $C_{28}H_{32}FN_4O_{12}$ 635.2: found 635.1.

CO-GlcN-1. The acetylated glucosamine derivative **9** was stirred in 75% MeOH in H_2O with 4.5 eq. of K_2CO_3 for 30 min. The base was neutralized with Dowex 50WX8 H$^+$, filtered and rinsed with MeOH, and the MeOH was removed under reduced pressure. The resulting residue was purified by reverse-phase HPLC using a flow rate of 2 mL min^{-1} with the following gradient where H_2O (0.2% TFA) is solvent A and CH_3CN is solvent B: 0–5 min 20% B, 15 min 35% B, 25 min 40% B, 35 min 85% B, providing the compound as the hydro trifluoroacetate (contains mixture of α and β anomers), 6.3 mg, 0.0109 mg, 6% yield. **^{1}H NMR** (600.27 MHz, D_2O) δ 3.14 (dd, J = 8.3, 10.9 Hz, 0.2 H), 3.39 (dd, J = 3.4, 10.5 Hz, 0.8 H), 3.48 (dd, J = 9.0, 10.2 Hz, 1 H), 3.53 (ddd, J = 1.9, 5.6, 9.8 Hz, 0.2 H), 3.76 (m, 1 H), 3.82–3.94 (m, 2 H), 4.03 (dd, J = 9.0, 10.5 Hz, 0.8 H), 4.23–4.40 (m, 1 H), 4.40–4.54 (m, 1 H), 4.86 (m, 2 H), 5.13 (d, J = 8.3 Hz, 0.2 H), 5.68 (d, J = 3.8 Hz, 0.8 H), 6.93–7.09 (m, 2 H), 7.71 (d, J = 8.7 Hz, 1 H), 8.47 (s, 1 H), 8.58–8.73 (m, 1 H); **^{13}C NMR** (150.94 MHz, D_2O) δ 39.7, 41.0, 59.4, 60.2, 60.4, 61.6, 68.1 (d, $^2J_{C-F}$ = 18.6 Hz), 69.5, 69.7, 70.0, 71.3, 76.1, 82.3 (d, $^1J_{C-F}$ = 164.6 Hz), 87.9, 92.4, 101.4, 111.8, 114.4, 115.3, 117.3, 119.5, 127.2, 127.4, 130.9, 137.9, 138.0, 138.30, 138.33, 154.6, 158.5, 162.8, 163.1; **^{19}F NMR** (564.82 MHz, D_2O) δ −78.5 (TFA), −226.30 (ttt); **HRMS** (ESI) m/z: [M + H]$^+$ calcd for $C_{20}H_{23}FN_4O_8$

467.1573: found 467.1575; **UV/Vis** (PBS pH 7.4): absorbance λ_{max} (ε): 340 nm (12 000 L mol^{-1} cm^{-1}); fluorescence λ_{max}: 420 nm (340 nm excitation).

Ethyl 7-(2-fluoroethoxy)-2-oxo-2*H*-chromene-3-carboxylate. Ethyl 7-hydroxy-2-oxo-2*H*-chromene-3-carboxylate (0.545 mmol), which was synthesized according to a literature procedure,[46] and K_2CO_3 (0.818 mmol) was suspended in DMF (1.2 mL) and flushed with N_2. This was stirred at 70 °C for 10 min. Then 1-fluoro-2-iodoethane (0.818 mmol) was added dropwise, and the reaction was stirred at 70 °C for 6 h. The reaction mixture was diluted with EtOAc and washed with sat. $NaHCO_3$, and brine. The organic phase was concentrated, and the crude was recrystallized from EtOAc/hexane to provide white crystalline needles, 103.7 mg, 0.370 mmol, 68% yield. **^{1}H NMR** (399.978 MHz, $CDCl_3$) δ 1.40 (t, J = 7.1 Hz, 3 H), 4.24–4.29 (m, 1 H), 4.31–4.36 (m, 1 H), 4.40 (q, J = 7.1 Hz, 2 H), 4.71–4.77 (m, 1 H), 4.84–4.89 (m, 1 H), 6.83 (d, J = 2.4 Hz, 1 H), 6.94 (dd, J = 2.4, 8.7 Hz, 1 H), 7.52 (d, J = 8.7 Hz, 1 H), 8.50 (d, J = 0.6 Hz, 1 H).**^{13}C NMR** (175.976 MHz, $CDCl_3$) δ 14.2, 61.7, 67.8 (d, $^2J_{C-F}$ = 20.9 Hz), 81.3 (d, $^1J_{C-F}$ = 171.9 Hz), 101.0, 112.0, 113.9, 114.6, 130.8, 148.8, 157.0, 157.4, 163.3, 163.7. **^{19}F NMR** (376.318 MHz, $CDCl_3$) δ −223.84 (tt); **LRMS** (ESI) m/z: $[M + H]^+$ calcd for $C_{14}H_{14}O_5F$ 281.1; found 281.1.

7-(2-Fluoroethoxy)-2-oxo-2*H*-chromene-3-carboxylic acid (11). Ethyl 7-(2-fluoroethoxy)-2-oxo-2*H*-chromene-3-carboxylate (0.187 mmol) was suspended in 0.3 mL of 2 : 1 EtOH/H_2O (v/v), and NaOH (0.845 mmol) was added. This was immediately refluxed for 15 min, then cooled to rt. The reaction mixture was added dropwise to 0.6 mL of 20% HCl (~6.7 M) and cooled to 0 °C. The precipitate was filtered and washed with cold water, providing a pale yellow solid, 36.1 mg, 0.143 mmol, 77% yield. **^{1}H NMR** (399.980 MHz, $(CD_3)_2SO$) δ 4.40 (dt, J = 3.8, 30.0 Hz, 2 H), 4.68–4.87 (m, 2 H), 7.01–7.10 (m, 2 H), 7.84 (d, J = 8.6 Hz, 1 H), 8.72 (s, 1 H); **^{13}C NMR** (175.976 MHz, $(CD_3)_2SO$) δ 68.1 (d, $^2J_{C-F}$ = 18.4 Hz), 81.8 (d, $^1J_{C-F}$ = 167.4 Hz), 100.9, 111.9, 113.6, 114.1, 131.7, 149.0, 156.8, 157.2, 163.4, 164.1; **^{19}F NMR** (376.318 MHz, $(CD_3)_2SO$) δ −222.35 (tt); **LRMS** (ESI) m/z: $[M + H]^+$ calcd for $C_{12}H_{10}O_5F$ 253.1; found 253.1.

CO-GlcN-2. Compound **11** (0.0649 mmol), glucosamine·HCl (0.0974 mmol), and DIPEA (0.1974 mmol) was dissolved in DMF (0.22 mL). HBTU (0.0974 mmol) was added and the flask was flushed with N_2. The reaction was stirred overnight at rt. The crude mixture was diluted with 5.78 mL of 50/50 CH_3CN/0.2% TFA water, purified by reverse-phase HPLC using a flow rate of 2 mL min^{-1} with the following gradient where H_2O (0.2% TFA) is solvent A and CH_3CN is solvent B: 0–9 min 1% B, 25 min 60% B, 32 min 75% B, then lyophilized to give a fluffy white solid, 19.8 mg, 0.0479 mmol, 74% yield. **^{1}H NMR** (399.978 MHz, CD_3OD) δ 3.37–4.12 (m, 6 H), 4.31–4.36 (m, 1 H), 4.38–4.44 (m, 1 H), 4.67–4.74 (m, 1 H, second proton signal obscured by HDO) 5.19 (d, J = 3.5 Hz, 1 H), 7.02–7.09 (m, 2 H), 7.77 (d, J = 8.6 Hz, 1 H), 8.83 (d, J = 0.7 Hz, 1 H); **^{13}C NMR** (175.976 MHz, CD_3OD) δ 56.2, 62.8, 69.6 (d, $^2J_{C-F}$ = 19.8 Hz), 72.3, 73.3, 73.6, 82.8 (d, $^1J_{C-F}$ = 169.5 Hz), 92.6, 102.0, 114.0, 115.4, 115.8, 132.7, 149.6, 158.1, 162.9, 164.4, 165.6; **^{19}F NMR** (376.318 MHz, CD_3OD) δ −77.09 (s, TFA), −225.60 (tt); **HRMS** (ESI) m/z: $[M + Na]^+$ calcd for $NaC_{18}H_{20}O_9NF$ 436.1014: found 436.1013; **UV/Vis** (0.1% DMSO in Krebs–Ringer buffer pH 7.4): absorbance λ_{max} (ε): 350 nm (26 000 L mol^{-1} cm^{-1}); fluorescence λ_{max}: 400 nm (350 nm excitation).

7-Fluoro-2,1,3-benzoxadiazole-4-sulfonyl chloride (CBDF). Synthesized from 4-fluoro-2,1,3-benzoxadiazole (**16**) according to the literature procedure with slight modifications.[30] The crude was purified by flash column chromatography using 1 : 1 toluene/hexanes as eluent, providing an off-white solid, 384 mg, 1.63 mmol, 86% yield. R_f (1 : 1 toluene/hexanes) = 0.32; **^{1}H NMR** (498.12 MHz, $(CH_3)_2CO$) δ 7.70 (dd, J = 8.0, 9.0 Hz, 1 H), 8.60 (dd, J = 4.0, 8.0 Hz, 1 H); **^{13}C NMR** (125.69 MHz, $(CH_3)_2CO$) δ 114.5 (d, $^2J_{C-F}$ = 18.9 Hz), 128.7 (d, $^3J_{C-F}$ = 5.7 Hz), 139.9 (d, $^3J_{C-F}$ = 9.3 Hz), 144.6 (d, $^2J_{C-F}$ = 20.4 Hz), 146.7 (d, J = 3.1 Hz), 155.9 (d, $^1J_{C-F}$ = 276.0 Hz); **^{19}F NMR** (468.64 MHz, $(CH_3)_2CO$) δ −107.71 (dd, J = 3.7, 8.9 Hz); **HRMS** (EI) m/z: $[M]^+$ calcd for $C_6H_2ClFN_2O_3S$ 235.9459: found 235.9459.

7-Fluoro-2,1,3-benzoxadiazole-4-sulfonyl fluoride (FBDF). Synthesis was adapted from Dong *et al.*[31] A solution of KHF_2 (29.8 mg, 0.381 mmol) in H_2O (0.16 mL) was added to a solution of **17** (39.2 mg, 0.166 mmol) dissolved in CH_3CN (0.16 mL). This was then vigorously stirred for 2 h at rt. The reaction was then extracted with CH_2Cl_2 and washed with water then brine. The organic layer was dried with Na_2SO_4, filtered, and concentrated to provide pale white/yellow crystals, 36.5 mg, 0.166 mmol, >99% yield. R_f (1 : 1 EtOAc/hexanes) = 0.65; **^{1}H NMR** (498.12 MHz, $CDCl_3$) δ 7.32 (ddd, J = 1.0, 7.8, 8.5 Hz, 1 H), 8.33 (ddd, J = 0.8, 3.9, 7.8 Hz, 1 H); **^{13}C NMR** (125.69 MHz, $CDCl_3$) δ 112.5 (d, $^2J_{C-F}$ = 18.3 Hz), 118.7 (dd, J_{C-F} = 6.2 Hz, 32.5 Hz), 139.0 (dd, J_{C-F} = 2.1, 8.5 Hz), 142.8 (d, J_{C-F} = 19.8 Hz), 146.1 (d, J_{C-F} = 1.2, 2.8 Hz), 155.3 (d, $^1J_{C-F}$ = 281.1 Hz); **^{19}F NMR** (468.64 MHz, $CDCl_3$) δ −102.99 (dd, J = 3.7, 8.4 Hz), 63.97 (s); **HRMS** (EI) m/z: $[M]^+$ calcd for $C_6H_2F_2N_2O_3S$ 219.9754: found 219.9753.

Compound 2-FBDG. FBDF (13 mg, 0.059 mmol), D-glucosamine (free base, 16 mg, 0.089 mmol), and $NaHCO_3$ (7.5 mg, 0.089 mmol) was dissolved in DMF (0.5 mL) and stirred at rt overnight. The solvent was removed by reduced pressure evaporation. The crude was purified by reverse-phase HPLC using a flow rate of 2 mL min^{-1} with the following gradient where H_2O (0.2% TFA) is solvent A and CH_3CN is solvent B: 0–5 min 20% B, 10 min 35% B, 20 min 50% B, 32 min 84% B, then lyophilized, providing a yellow solid, 22 mg, 0.058 mmol, 99% yield. R_f (20% MeOH/EtOAc) = 0.57/0.65; **^{1}H NMR** (599.93 MHz, CD_3CN/D_2O) mixture of α/β δ 3.32–3.88 (m, 6 H), 4.78 (d, J = 7.8 Hz, 0.4 H), 5.26 (d, J = 2.9 Hz, 0.6 H), 6.58 and 6.60 (d, J = 8.5 Hz, 1 H), 6.99 (br s, 1 H), 7.46 (br d, J = 8.8 Hz), 8.13 and 8.14 (d, J = 8.5 Hz, 1 H); **^{13}C NMR** (125.69 MHz, CD_3CN) δ 62.6/62.7, 71.8, 72.9, 73.7, 76.0, 77.3, 91.5, 96.7, 101.2 (d, $^2J_{C-F}$ = 29.3 Hz), 101.6, 144.2, 145.4/145.6, 146.7/146.9; **^{19}F NMR** (468.64 MHz, CD_3CN) δ 64.21 (s), 64.28 (s); **HRMS** (ESI) m/z: $[M - H]^-$ calcd for $C_{12}H_{13}FN_3O_8S$ 378.0413: found 378.0411; **UV/Vis** (Krebs–Ringer buffer pH 7.4): absorbance λ_{max} (ε): 425 nm (16 400 L mol^{-1} cm^{-1}); fluorescence: λ_{max} = 570 nm (425 nm excitation).

Radiochemistry

N.c.a. [^{18}F]F$^-$ was produced *via* the ^{18}O(p,n)^{18}F nuclear reaction from [^{18}O]H_2O (Rotem Industries Ltd, Hyox ^{18}O-enriched water, min. 98%) on an ACSI TR19/9 Cyclotron (Advanced Cyclotron Systems Inc., Richmond, Canada). Cyclotron-produced [^{18}F]F$^-$ (~1 GBq) was trapped on a Waters SepPak® light QMA anion exchange cartridge. [^{18}F]CsF was eluted from the anion exchange cartridge using 300 μL of aqueous Cs_2CO_3 (10 mg mL^{-1}). 100 μL of the [^{18}F]CsF solution was added to a solution of **CBDF** (0.2 mg) in *t*-BuOH (100 μL) in an Eppendorf tube, and incubated for 5 min to form **[^{18}F]FBDF**. The reaction was added to an Eppendorf tube containing a solution of glucosamine (free base, 1.5 mg) and $NaHCO_3$ (1.5 mg) in DMF (500 μL). The vial was rinsed with an additional 100 μL of DMF to ensure complete transfer of **[^{18}F]FBDF**. The reaction is shaken vigorously at rt for 20 min, gradually turning a bright yellow color. The crude **2-[^{18}F]FBDG** was then diluted with 200 μL of distilled H_2O and purified by reverse-phase HPLC at a constant flow rate of 3 mL min^{-1} using the following gradient where H_2O is solvent A and CH_3CN is solvent B: 0–4.25 min 20% B, 7.5 min 35% B, 13 min 50% B, 20 min 84% B, t_R = 15.0 and 15.7 min (α and β anomer). **2-[^{18}F]FBDG** accounted for 83 ± 9% of the crude reaction mixture. The **2-[^{18}F]FBDG** peak was fractionated, isolated using a rotary evaporator, and reformulated in 200 μL saline (60–80 MBq **2-[^{18}F]FBDG** final activity). RCY was 69 ± 3% (n = 3) d.c. over 2 steps.

Quality control was performed using thin layer chromatography (TLC) on silica plates using 10% EtOH/EtOAc as mobile phase (R_f ([^{18}F]FBDG) = 0.47, 100% radiochemical purity) and analytical Radio-HPLC using a gradient of MeCN (B)/H_2O (A) 0–3 min 10% B, 10 min 30% B, 17 min 50% B, 23 min 70% B, 27–30 min 90% B, 1 mL min^{-1} (t_R = 17.0 and 17.8 min, 95.8% purity).

In vitro 2-[^{18}F]FDG competition assay

EMT6 cells were seeded in 12-well plates at 100 000 cells per well 24 hours before the competition assay. 1 h before the assay, the cell media was removed, and the cells were rinsed with pH 7.4 PBS twice. The cells were then incubated at 37 °C with 1 mL of Krebs buffer. Then the buffer was aspirated, and the cells were treated with various concentrations of the non-radioactive dual-probes as well as a constant amount of **2-[^{18}F]FDG** per well (~0.111 MBq per well) – the total treatment volume was 300 μL (in Krebs buffer (pH 7.4)). The cells were incubated for 1 h at 37 °C. After incubation, the treatment was removed, and the cells were rinsed with ice-cold PBS twice. 400 μL of RIPA was added to each well to lyse the cells for at least 10 min. After cell lysis, 300 μL of the cell lysate was pipetted into scintillation vials for activity using a 2480 automatic gamma counter WIZARD2 (PerkinElmer, Waltham, MA, USA). These experiments were also repeated using D-glucose and 2-NBDG as reference compounds.

Confocal microscopy experiments with 2-FBDG in EMT6 and MDA-MB231 cells

The procedure was adapted from Soueidan *et al.*[47] EMT6 or MDA-MB231 cells were grown on coverslips to ~90% confluency. 1 h before the assay, the cell media was removed, and the cells were rinsed with pH 7.4 PBS twice. The cells were then incubated at 37 °C with 1 mL of Krebs buffer. The buffer was aspirated, and the cells were treated with 1 mL of either 200 μM **2-FBDG** or 200 μM **2-FBDG** + 50 μM D-glucose (in pH 7.4 Krebs buffer) for 1 h at 37 °C. The treatment was aspirated, then the cells were washed with ice-cold PBS twice. The cells were then incubated for 7 min at rt with 1 mL of 3.5% PFA in PBS. After PFA removal, the cells were permeabilized using 1 mL of 0.02% Triton X-100 in PBS for 5 min. The permeabilizing solution was removed and the cells were washed with PBS. Then the cells were treated with 1 mL of 0.3 μmol mL^{-1} DAPI in PBS for 15 min. The DAPI solution was removed and the cells were rinsed with PBS. The coverslips were then mounted onto microscopy slides using 15 μL of Mowiol. The slides were then imaged using the same settings on the Leica SP8 Falcon STED.

Dynamic PET imaging experiments

All animal experiments were carried out in accordance with guidelines of the Canadian Council on Animal Care and approved by the local animal care committee of the Cross Cancer Institute. The procedure was performed on MDA-MB-231 tumor-bearing BALB/c mice according to Wuest *et al.*[32] PET imaging of **2-[^{18}F]FBDG** was performed on an INVEON PET/CT scanner (Siemens Preclinical Solutions, Knoxville, TN, USA). Prior to radiotracer injection, mice were anesthetized through inhalation of isoflurane in 40% oxygen/60% nitrogen (gas flow 1 L min^{-1}), and body temperature was kept constant at 37 °C. Mice were placed in a prone position into the center of the field of view. A transmission scan for attenuation correction was not acquired. Mice were injected with 5 MBq of **2-[^{18}F]FBDG** or 5 MBq of **2-[^{18}F]FDG** in 150 μL of isotonic saline solution (0.9% w/v of NaCl) through a tail vein catheter. Data acquisition was performed over 60 min in 3D list mode. The dynamic list mode data were sorted into sinograms with 54 time frames (10 × 2, 8 × 5, 6 × 10, 6 × 20, 8 × 60, 10 × 120, 6 × 300 s). The frames were reconstructed using maximum a posteriori (MAP) as reconstruction mode. No correction for partial volume effects was applied. The image files were processed using the ROVER v2.0.51 software (ABX GmbH, Radeberg, Germany). Masks defining 3D regions of interest (ROI) were set, and the ROIs were defined by thresholding. ROIs covered all visible tumor mass of the subcutaneous tumors, and the thresholds were defined by 50% of the maximum radioactivity uptake level. Mean standardized uptake values [SUV_{mean} = (activity/mL tissue)/(injected activity/body weight), mL g^{-1}] were calculated for each ROI, and time-activity curves (TAC) were generated. All semiquantified PET data are presented as means ± SEM. Statistical differences were tested by Student's t test and were considered significant for $P < 0.05$.

Metabolic stability studies *in vivo*

The procedure was performed according to Richter *et al.*[48] For metabolic stability studies *in vivo*, normal BALB/c mice were

anesthetized through inhalation of isoflurane in 40% oxygen/60% nitrogen (gas flow 1 L min^{-1}) prior to i.v. injection of 25 MBq [^{18}F]FBDG *via* the tail vein. Venous blood samples were collected at 5, 15, 30, and 60 min p.i. *via* the mouse tail vein and further processed. Blood cells were separated by centrifugation (13 000 rpm × 5 min). Supernatant was removed, and the contained proteins were precipitated by addition of 2 volume parts of methanol (2 vol of MeOH/1 vol of sample).

Another centrifugation step (13 000 rpm × 5 min) was performed to obtain the plasma in the supernatant. The clear plasma supernatant was injected onto a Shimadzu HPLC system. The samples were analyzed using a Phenomenex Luna 10u C18(2) 100A, 250 × 4.6 mm column at a constant flow rate of 1 mL min^{-1}, and the following gradient with H_2O as solvent A and CH_3CN as solvent B: 0–3 min 10% B, 10 min 30% B, 17 min 50% B, 23 min 70% B, 27–30 min 90% B.

Conflicts of interest

There are no conflicts to declare.

Acknowledgements

The authors thank Floyd Baker, David Clendening, and Blake Lazurko from the Edmonton Radiopharmaceutical Center for ^{18}F production on a TR-19 cyclotron (Advanced Cyclotron Systems Inc, Vancover, BC, Canada). And Joanne D. Smith (Dept. of Oncology, University of Alberta) for her assistance with the confocal imaging. The authors are also grateful to Dan McGinn (Vivarium of the Cross Cancer Institute, Edmonton, AB, Canada) for supporting the animal work and Dr Hans-Soenke Jans (University of Alberta) for technical help and support of the preclinical PET facility as well as the Dianne and Irving Kipnes Foundation for supporting this work.

References

1 T. Hussain and Q. T. Nguyen, *Adv. Drug Delivery Rev.*, 2014, **66**, 90–100.
2 F. F. An, M. Chan, H. Kommidi and R. Ting, *AJR, Am. J. Roentgenol.*, 2016, **207**, 266–273.
3 M. A. Klenner, G. Pascali, M. Massi and B. H. Fraser, *Chem. – Eur. J.*, 2021, **27**, 861–876.
4 F. L. Thorp-Greenwood and M. P. Coogan, *Dalton Trans.*, 2011, **40**, 6129–6143.
5 S. M. Ametamey, M. Honer and P. A. Schubiger, *Chem. Rev.*, 2008, **108**, 1501–1516.
6 S. Lee and X. Chen, *Mol. Imaging*, 2009, **8**, 87–100.
7 A. Azhdarinia, P. Ghosh, S. Ghosh, N. Wilganowski and E. M. Sevick-Muraca, *Mol. Imaging Biol.*, 2012, **14**, 261–276.
8 S. Lütje, M. Rijpkema, W. Helfrich, W. J. Oyen and O. C. Boerman, *Mol. Imaging Biol.*, 2014, **16**, 747–755.
9 D. Li, J. Zhang, C. Chi, X. Xiao, J. Wang, L. Lang, I. Ali, G. Niu, L. Zhang, J. Tian, N. Ji, Z. Zhu and X. Chen, *Theranostics*, 2018, **8**, 2508–2520.
10 Q. T. Nguyen and R. Y. Tsien, *Nat. Rev. Cancer*, 2013, **13**, 653–662.
11 D. Hanahan and R. A. Weinberg, *Cell*, 2011, **144**, 646–674.
12 R. S. Brown and R. L. Wahl, *Cancer*, 1993, **72**, 2979–2985.
13 R. Paul, R. Johansson, P. L. Kellokumpu-Lehtinen, K. O. Söderström and L. Kangas, *Res. Exp. Med.*, 1985, **185**, 87–94.
14 L. Speizer, R. Haugland and H. Kutchai, *Biochim. Biophys. Acta*, 1985, **815**, 75–84.
15 Y. Cheng, G. Shabir, X. Li, L. Fang, L. Xu, H. Zhang and E. Li, *Chem. Commun.*, 2020, **56**, 1070–1073.
16 H. Xu, X. Liu, J. Yang, R. Liu, T. Li, Y. Shi, H. Zhao and Q. Gao, *Biochem. Biophys. Res. Commun.*, 2016, **474**, 240–246.
17 A. Jo, J. Sung, S. Lee, H. Nam, H. W. Lee, J. Park, H. M. Kim, E. Kim and S. B. Park, *Bioconjugate Chem.*, 2018, **29**, 3394–3401.
18 R. A. Sheth, L. Josephson and U. Mahmood, *J. Biomed. Opt.*, 2009, **14**, 064014–064014.
19 B. L. Cox, T. R. Mackie and K. W. Eliceiri, *Am. J. Nucl. Med. Mol. Imaging*, 2014, **5**, 1–13.
20 X. Tong, A. Garofalakis, A. Dubois, R. Boisgard, F. Ducongé, R. Trébossen and B. Tavitian, *EJNMMI Res.*, 2012, **2**, 19.
21 Y.-D. Kwon, Y. Byun and H.-K. Kim, *Nucl. Med. Biol.*, 2021, **93**, 22–36.
22 L. Sun, J. Ding, W. Xing, Y. Gai, J. Sheng and D. Zeng, *Bioconjugate Chem.*, 2016, **27**, 1200–1204.
23 V. G. Ostapchenko, J. Snir, M. Suchy, J. Fan, M. R. Cobb, B. A. Chronik, M. Kovacs, V. F. Prado, R. H. E. Hudson, S. H. Pasternak, M. A. M. Prado and R. Bartha, *Contrast Media Mol. Imaging*, 2019, **2019**, 6403274.
24 W. L. Turnbull, L. Yu, E. Murrell, M. Milne, C. L. Charron and L. G. Luyt, *Org. Biomol. Chem.*, 2019, **17**, 598–608.
25 W. L. Turnbull, E. Murrell, M. Bulcan-Gnirss, M. Majeed, M. Milne and L. G. Luyt, *Dalton Trans.*, 2019, **48**, 14077–14084.
26 W. Song, Y. Wang, J. Qu and Q. Lin, *J. Am. Chem. Soc.*, 2008, **130**, 9654–9655.
27 Z. Li, L. Qian, L. Li, J. C. Bernhammer, H. V. Huynh, J. S. Lee and S. Q. Yao, *Angew. Chem., Int. Ed.*, 2016, **55**, 2002–2006.
28 K. Sivakumar, F. Xie, B. M. Cash, S. Long, H. N. Barnhill and Q. Wang, *Org. Lett.*, 2004, **6**, 4603–4606.
29 V. V. Rostovtsev, L. G. Green, V. V. Fokin and K. B. Sharpless, *Angew. Chem., Int. Ed.*, 2002, **41**, 2596–2599.
30 T. Toyo'oka and K. Imai, *Anal. Chem.*, 1984, **56**, 2461–2464.
31 J. Dong, L. Krasnova, M. G. Finn and K. B. Sharpless, *Angew. Chem., Int. Ed.*, 2014, **53**, 9430–9448.
32 M. Wuest, I. Hamann, V. Bouvet, D. Glubrecht, A. Marshall, B. Trayner, O. M. Soueidan, D. Krys, M. Wagner, C. Cheeseman, F. West and F. Wuest, *Mol. Pharmacol.*, 2018, **93**, 79–89.

33 I. Hamann, D. Krys, D. Glubrecht, V. Bouvet, A. Marshall, L. Vos, J. R. Mackey, M. Wuest and F. Wuest, *FASEB J.*, 2018, **32**, 5104–5118.
34 A. Brito, P. M. R. Pereira, D. S. de Costa, R. L. Reis, R. V. Ulijin, J. S. Lewis, R. A. Pires and I. Pashkuleva, *Chem. Sci.*, 2020, **11**, 3737–3744.
35 J. A. Inkster, K. Liu, S. Ait-Mohand, P. Schaffer, B. Guérin, T. J. Ruth and T. Storr, *Chem. – Eur. J.*, 2012, **18**, 11079–11087.
36 F. D. Grant, F. H. Fahey, A. B. Packard, R. T. Davis, A. Alavi and S. T. Treves, *J. Nucl. Med.*, 2008, **49**, 68–78.
37 D. Ory, J. Van den Brande, T. de Groot, K. Serdons, M. Bex, L. Declercq, F. Cleeren, M. Ooms, K. Van Laere, A. Verbruggen and G. Bormans, *J. Pharm. Biomed. Anal.*, 2015, **111**, 209–214.
38 G. Pascali, L. Matesic, B. Zhang, A. T. King, A. J. Robinson, A. T. Ung and B. H. Fraser, *EJNMMI Radiopharm. Chem.*, 2017, **2**, 9.
39 L. Matesic, N. A. Wyatt, B. H. Fraser, M. P. Roberts, T. Q. Pham and I. Greguric, *J. Org. Chem.*, 2013, **78**, 11262–11270.
40 A. Narayanan and L. H. Jones, *Chem. Sci.*, 2015, **6**, 2650–2659.
41 R. Schirrmacher, G. Bradtmöller, E. Schirrmacher, O. Thews, J. Tillmanns, T. Siessmeier, H. G. Buchholz, P. Bartenstein, B. Wängler, C. M. Niemeyer and K. Jurkschat, *Angew. Chem., Int. Ed.*, 2006, **45**, 6047–6050.
42 C. W. Harwig, R. Ting, M. J. Adam, T. J. Ruth and D. M. Perrin, *Tetrahedron Lett.*, 2008, **49**, 3152–3156.
43 Z. Qinheng, X. Hongtao, W. Hua, D. Wen-Ge Han, W. Nan, X. Huan, G. Yuang, N. Louis, Y. Guang, S. K. Barry and W. Peng, [18F]SuFEx Click Chemistry Enabled Ultrafast Late-stage Radiosynthesis, *ChemRxiv*, 2020.
44 I. Suketaka, T. Yumo and K. Akikazu, *Bull. Chem. Soc. Jpn.*, 1976, **49**, 762–766.
45 S. Masuko, S. Bera, D. E. Green, M. Weïwer, J. Liu, P. L. DeAngelis and R. J. Linhardt, *J. Org. Chem.*, 2012, **77**, 1449–1456.
46 L. C. C. Vieira, M. W. Paixão and A. G. Corrêa, *Tetrahedron Lett.*, 2012, **53**, 2715–2718.
47 O. M. Soueidan, T. W. Scully, J. Kaur, R. Panigrahi, A. Belovodskiy, V. Do, C. D. Matier, M. J. Lemieux, F. Wuest, C. Cheeseman and F. G. West, *ACS Chem. Biol.*, 2017, **12**, 1087–1094.
48 S. Richter, M. Wuest, C. N. Bergman, S. Krieger, B. E. Rogers and F. Wuest, *Mol. Pharm.*, 2016, **13**, 1347–1357.